Current Problems in Diagnostic Radiology 48 (2019) 152–160

Current Problems in Diagnostic Radiology

journal homepage: www.cpdrjournal.com

Breathe New Life Into Your Chest CT Exams: Using Advanced Acquisition and Postprocessing Techniques

Nikkole M. Weber, RT (R)[a], Chi Wan Koo, MD[a], Lifeng Yu, PhD[a], Brian J. Bartholmai, MD[a], Ahmed F. Halaweish, PhD[b], Cynthia H. McCollough, PhD[a], Joel G. Fletcher, MD[a,*]

[a] *Department of Radiology, Mayo Clinic, Rochester, MN.*
[b] *Siemens Healthineers, Malvern, PA.*

A B S T R A C T

Objective: Chest computed tomography (CT) imaging enables detailed visualization of the pulmonary structures and diseases. This article reviews how continued innovation and improvements in modern CT system hardware and software now facilitate a wider range of image acquisition options and generate unique qualitative and quantitative information that can benefit patients

Results: Dual energy imaging utilizes two x-ray energies to highlight differences in tissue properties and increase iodine signal to improve diagnosis or reduce metal artifacts. Ultra-low dose imaging can be performed by using additional x-ray beam filtration, such as a tin filter, combined with iterative reconstruction algorithms to benefit lung cancer screening or pediatric imaging. Ultra-fast pitch spiral acquisition improves temporal resolution and reduces motion artifacts. Higher spatial resolution acquisition and reconstruction methods permit improved visualization of small structures. Radiomic analysis of chest CT image features permits risk stratification of pulmonary nodules and masses and reliable measures of change in pulmonary architecture and disease.

Conclusions: Multiple new CT acquisition and reconstruction techniques, along with advanced post processing methods permit detailed analysis of changes in pulmonary architecture and function, and an expanded ability to adapt chest CT to the unique needs of different patients.

Introduction

A thoracic computed tomography (CT) scan is one of the most common diagnostic examinations in a busy radiology department, with clinical indications encompassing lung cancer screening and staging, pulmonary angiography and interstitial lung disease evaluation. Given recent innovations in CT technology, a wider spectrum of acquisition and postprocessing techniques are now available, which can be tailored individually to the patient and the particular diagnostic task at hand. Advanced acquisition techniques such as dual energy CT (DECT),[1,2] fast pitch acquisition,[3] and ultra-low-dose exams[4,5] offer beneficial options for different applications. Additionally, reconstruction parameter choices can have considerable qualitative and quantitative impact depending on postprocessing and display options needed in any particular practice. Postprocessing methods can reduce interobserver variability and provide quantitative information that cannot be determined visually and in a reliable fashion. The purpose of this review is to provide an overview of recent CT innovations that enable customization of CT exams so as to achieve the greatest benefit for each patient.

*Reprint requests: Joel G. Fletcher, MD, Department of Radiology, Mayo Clinic, 200 First Street SW, Rochester, MN 55905.
E-mail address: fletcher.joel@mayo.edu (J.G. Fletcher).

https://doi.org/10.1067/j.cpradiol.2018.10.003
0363-0188/

Advanced Acquisition Techniques

Dual energy CT is based on the fact that there are 2 major mechanisms responsible for attenuation of x-rays in the relevant diagnostic energy range of CT imaging: the photoelectric effect, which largely depends on the atomic number, and Compton scattering, which depends on electron density.[6] With dual energy measurements, it is possible to solve for the coefficients of the 2 effects (or 2 basis materials) if their atomic number differ substantially.[6] The quality and accuracy of dual energy-based material classification or quantification depends on the separation of the high and low kV spectra, with greater spectral separation resulting in improved classification and quantification.[6,7] Consequently, a tin filter (Sn) can be placed in front of a high energy x-ray beam to filter out low energy photons and increase spectral separation from a low energy tube. This arrangement is represented by stating the tube energy along with the atomic symbol representing the attenuating filter (eg, 140 kV/Sn).

Several parameters are adjusted in DECT scanning, with the ability to adjust these parameters depending on the CT hardware. For dual source CT, the kV pairs (or tube energy of each x-ray tube) are selected based on patient size, with image noise in the lower tube potential usually being the deciding factor. For example, on a second-generation dual-source CT scanner (Somatom Definition Flash, Siemens Healthineers), small patients can be imaged with a kV pair of 80 kV and 140 kV/Sn, while larger patients would be scanned with a

kV pair of 100 kV and 140 kV/Sn. Above a certain patient size (45 cm lateral dimension at the level of the liver in our practice), dual energy is not used, owing to excessive image noise in the low kV acquisition. On a single source CT system that uses either rapid kV switching or sandwich detectors to enable dual-energy acquisition, the 2 tube potentials or spectra are typically fixed by the scanner configuration.[2]

The pitch for DECT is chosen to reduce helical artifacts and nonuniform dose effects, and the rotation time is typically set to 0.5 seconds or less in order to reduce motion artifacts while still offering sufficient dose output. Radiation dose level is chosen to match analogous single energy CT examinations. For single and dual energy CT, reconstruction kernels are chosen to reflect the diagnostic task (eg, a softer kernel for mediastinal evaluation and a sharper kernel to evaluate nodules, bronchi and interstitial lung disease [Fig 1]), with sharper kernels displaying finer details but also having more image noise. Iterative reconstruction may be used to reduce image noise, particularly for lower dose examinations.

Ultrafast acquisition can be accomplished using wide CT detectors, fast tube rotation times, or high-pitch dual source mode (Fig. 2, and 3). In general, with the increase of the longitudinal detector coverage, the scanning speed becomes faster. One caveat of using a wide detector (eg, 16 cm) is that it may not be appropriate for helical scan due to the cone-beam effect.[8] On a dual-source CT scanner, a high-pitch scanning mode (pitch > 3) becomes possible because the 2 sources can acquire complementary data to fill in gaps for image reconstruction (Fig 2).[3] With a high-pitch scanning mode, the whole chest can be scanned within 1 second. Ultrafast acquisition is routinely used in our CT practice for pediatric (to avoid the use of anesthesia) and noncompliant patients (eg, those with tremors) as well as for pulmonary CT angiography to detect pulmonary embolism (Fig 3).[9,10] The trade off with ultrafast acquisition is that greater tube currents are required to decrease incremental image noise, and CT system limitations often result in increased streaking artifacts near the ribs despite lower motion artifacts (Fig 4).

Ultra low dose CT is used when radiation dose is a concern, such as multiple scans in high-risk patients without known disease (eg, lung cancer screening), pediatric patients, or those undergoing multiple surveillance CT exams. It is ideal for detecting small pulmonary nodules regardless of nodule attenuation. Acquisition approaches for ultra-low-dose exams include lowering the tube current or optimizing the x-ray beam spectrum (for example by adding a tin filter), and by compensating for increased image noise in image reconstruction using iterative reconstruction or other denoising algorithms. Figure 5 shows how the combination of various tube energies and tin filtration can be used to remove low energy photons that do not contribute to image formation, improving dose efficiency. These spectra were generated using a simulation tool (DRASIM, Siemens Healthcare).[11] The thickness of the tin filter used in this example was 0.6 mm, which

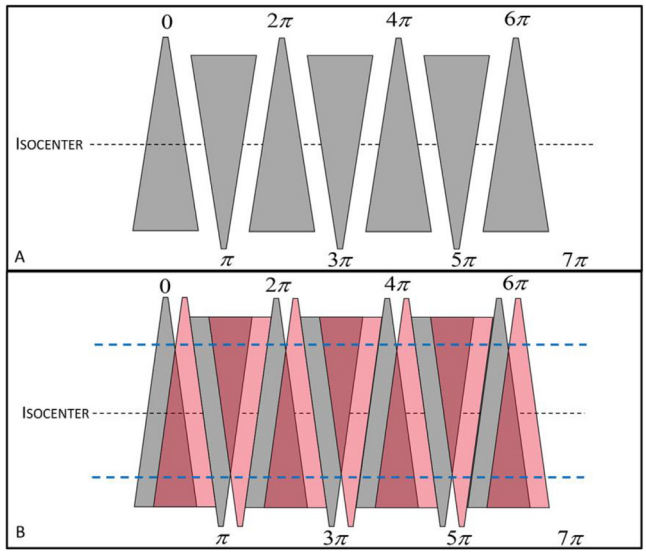

FIG 2. (A) Image depicts gaps in single source CT data as an x-ray source travels at a very high pitch (of 3.0), with grey triangles representing the x-ray beam and the white gaps representing gaps in the projection data. (B) Image depicting the ability of the dual source configuration to fill in complementary gaps at high pitch of 3.0 (with grey and pink triangles representing the x-ray beams of the 2 x-ray sources). Dual source scanning with ultrafast pitch is able to fill in the projection data gaps that are otherwise present using a single source approach. The blue dashed lines represent the field of view with complete projection data for image reconstruction.

(Courtesy of Siemens Healthineers, Malvern, PA). (Color version of figure is available online.)

was selected as a result of tradeoff between beam quality and radiation output. With a thicker tin filter, the beam becomes more hardened (mean energy shifted more to the right), but the radiation output becomes more reduced and may be for the patient. Therefore, the thickness of the tin filter has to be appropriately selected. With the tin filter, noise is reduced 46% at the same dose; conversely, if this noise reduction is translated to dose reduction, a dose reduction of 58% will keep the noise level constant (Fig 6). Figure 7 shows an example of a ground-glass nodule with a 90% dose reduction using 100 kV/Sn compared to routine low-dose chest CT at 120 kV, with similar conspicuity of the nodule between imaging techniques.

Spectral shaping using metal filters is not available on all scanners, and substantial dose reduction can be obtained by simply lowering automatic exposure control settings, with iterative reconstruction or another denoising algorithm employed to improve image quality.[12] Careful evaluation of the impact of iterative reconstruction and its strength setting is recommended before it is applied in chest CT. If the iterative reconstruction strength is too high, the noise texture

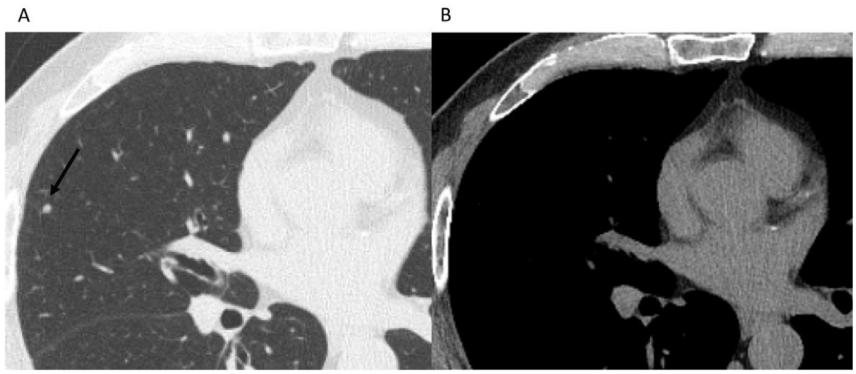

FIG 1. Sixty-three-year-old male underwent non-contrast CT to follow-up treatment of Chronic Lymphocytic Leukemia in relapse displaying a 4 mm indeterminate pulmonary nodule. A. 1 mm sharp kernel (Bv59) B. 1 mm soft tissue kernel (Br40). (A) Showing sharp kernel with lung window for the lung nodule and corresponding soft tissue window for mediastinum findings (B).

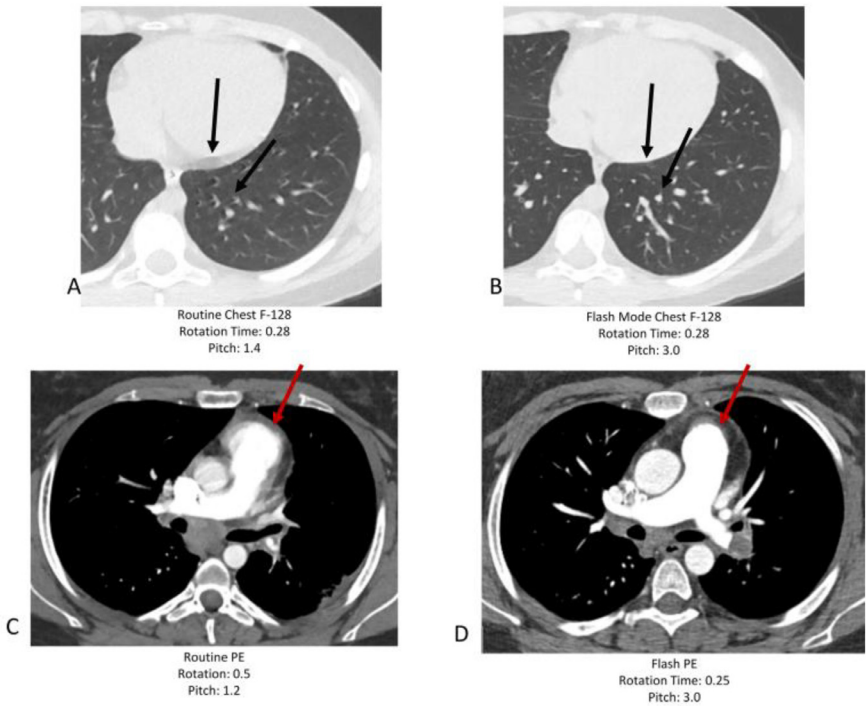

FIG 3. Fast-pitch scanning in routine clinical practice. (A) Axial non-contrast CT image using routine acquisition parameters (rotation time 0.28 seconds, pitch 1.4) in a 9-year-old female showing motion artifacts (arrows) most noticeable in the left lower lobe. Note ghosting of the bronchi, vessels and the heart. (B) High pitch scanning mode in the same patient. The bronchi and vessels of the lung as well as heart border are now well defined. Similar benefits of using a high pitch scanning mode can be seen when performing a CT angiogram for pulmonary embolism evaluation. Decreased motion artifact of the main pulmonary artery is demonstrated on images C and D (arrows). Routine acquisition parameters (rotation time 0.5 seconds, pitch 1.2) (C) vs a high-pitch scanning mode (rotation time 0.28 seconds, pitch 3) (D).

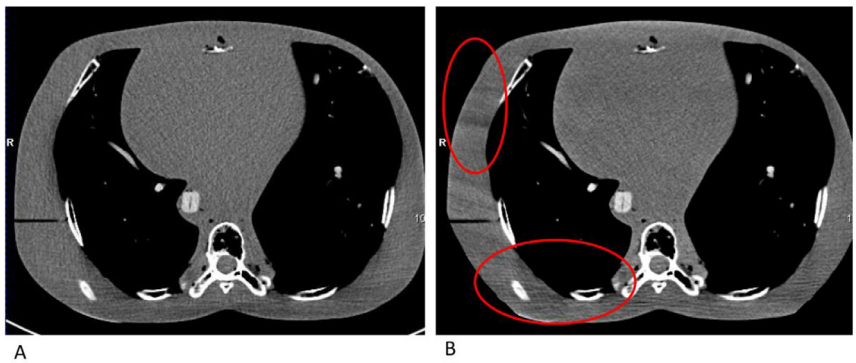

FIG 4. Helical and streaking artifacts at high-pitch scanning mode. (A) Routine-pitch, single source CT scan of an anthropomorphic phantom shows minimal helical and streaking artifacts. (B) High-pitch, dual source CT scan of the same phantom shows obvious helical and streaking artifacts in the right lateral and right posterior chest walls, mainly due to the use of high pitch.

may be altered excessively and could negatively affect the diagnostic confidence.[13]

Common and Advanced Image Reconstruction Techniques

Common image reconstruction parameters that need to be defined for every chest CT exam include reconstruction kernel, slice thickness, reconstruction increment, imaging plane, and average or maximum intensity projections. Reconstruction kernels suppress or enhance specific ranges of spatial frequencies to augment the visibility of certain features,[14,15] ultimately affecting the performance for lesion-detection tasks. The high-resolution algorithms preserve the higher spatial frequencies, rendering detailed visualization of the airways, lung markings and osseous structures. However, this is done at the expense of greater noise. On the other hand, soft tissue algorithms reduce the higher frequency contribution thus decreasing the noise but also reducing the spatial resolution. Such algorithms are employed for mediastinal structure evaluations where fine details are

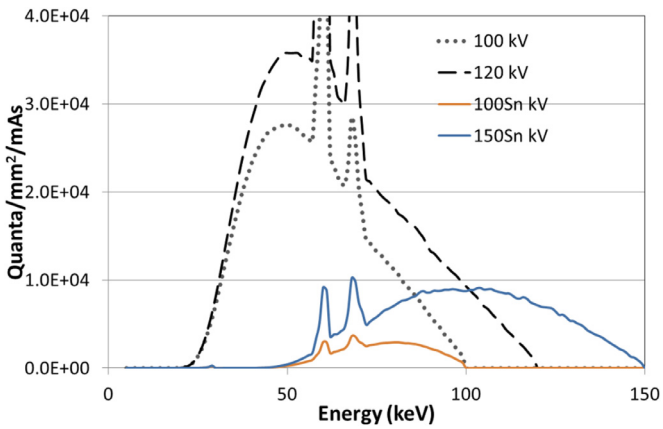

FIG 5. X-ray beam spectra of 100 kV, 120 kV, 100 kV plus a tin filter (100Sn), and 150 kV plus Sn filter (150Sn). The thickness of the tin filter was 0.6 mm to achieve a balance between beam quality and radiation output. With the added Sn filter, the radiation output per mAs is greatly reduced, but with a much harder beam quality.

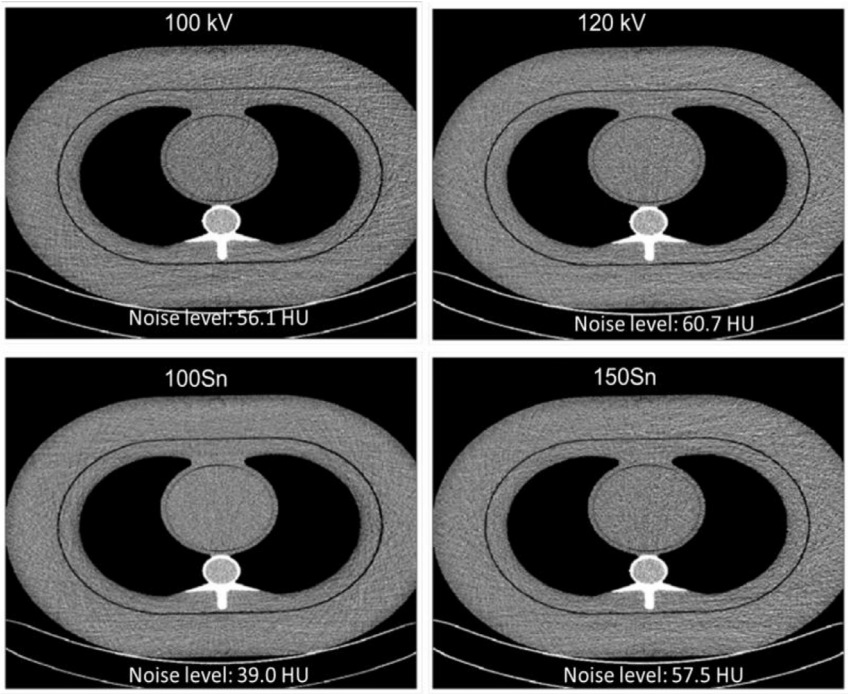

FIG 6. Phantom images acquired at different kV settings. Radiation output (CTDIvol) matched to a typical lung cancer screening technique: 120 kV, 25 Quality reference mAs, nominal CTDIvol 1.7 mGy. The 100Sn kV setting yields the lowest image noise, with noise measured over the heart region of the phantom.

not required generally. In order to maximize the benefits of both reconstruction kernels and interpretation efficiency, a hybrid or intermediate kernel is typically utilized in our institution. An intermediate kernel has been shown to be comparable to both the high resolution and soft tissue algorithm.[16] For nodule characterization, it is imperative to acquire thin thickness images in the order of 1-2 mm because solid nodules can be misrepresented as ground glass attenuation due to air-soft tissue volume averaging on thick slices. Similarly, multiplanar reformatted imaging is essential to differentiate flat lesions, such as a scar, and rounded lesions, such as a nodule or a mass (Fig 8).

One of the computer-aided nodule detection tools that has been successfully incorporated into most radiology practices is maximum intensity projection (MIP). According to several groups, MIP is the most sensitive reconstruction technique for detecting small pulmonary nodules, especially ones less than 5 mm (Fig 9).[17-19] Park et al conducted a large study of 514 nodules where they showed statistically significant improvements in nodule identification utilizing MIP and computer-aided detection (CAD).[20]

Several advanced reconstructions and postprocessing techniques are routinely used for DECT exams, including the mixed kV linear blend, virtual noncontrast virtual monoenergetic and perfused blood volume maps (Fig 10).[21] Dual energy imaging can increase iodine signal in several ways. Mixed kV linear blend images can be used to increase the weighting of image data corresponding to the low energy x-ray tube or acquisition, thereby accentuating iodine signal similar to low kV CT acquisition techniques.[22] Material classification

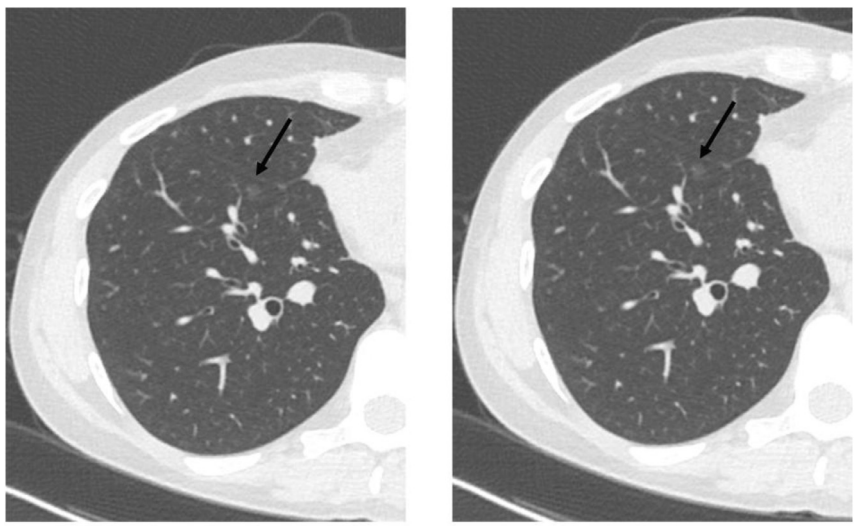

FIG 7. Forty-year-old male with a family history of lung cancer and now with a personal history of lung nodules. Both standard dose and ultra-low dose CT exams were performed. Note preservation of visibility and characteristics of a 7 mm pure ground glass nodule on the ultra-low dose image with 100 kV and tin filtration (A) compared to the routine 120 kV image (B).

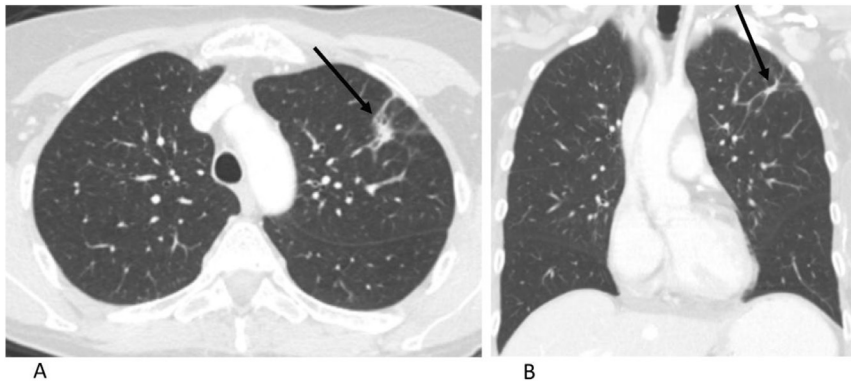

FIG 8. Sixty-two-year-old female presented for surveillance of recurrent anal cancer. A spiculated left upper lobe solid nodular density was found on axial CT (A), corresponding to a flat lesion on the coronal CT (B) and is therefore a scar as opposed to a lung nodule. This case illustrates the importance of multiplanar reformatted images in problem solving.

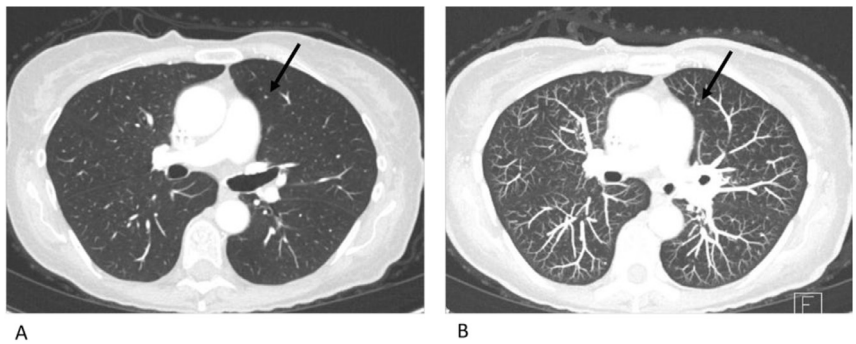

FIG 9. Sixty-three-year-old male scanned using a routine non-contrast chest technique. Cross-sectional reformatted images (A) axial thin images with a medium sharp kernel and (B) MIP axial images. Arrow points to a small pulmonary nodule.

uses CT attenuation information at each x-ray tube energy to characterize pixels into different materials, such as iodine, soft tissue, and water. "Virtual" noncontrast images then display the soft tissue and water information while "virtual" iodine images only display the corresponding iodine maps.[21,23] "Virtual" monoenergetic images can then be created corresponding to different individual keV settings, with lower keVs such as 40 and 50 keV accentuating iodine signal and contrast differences but also having more noise, and high keV

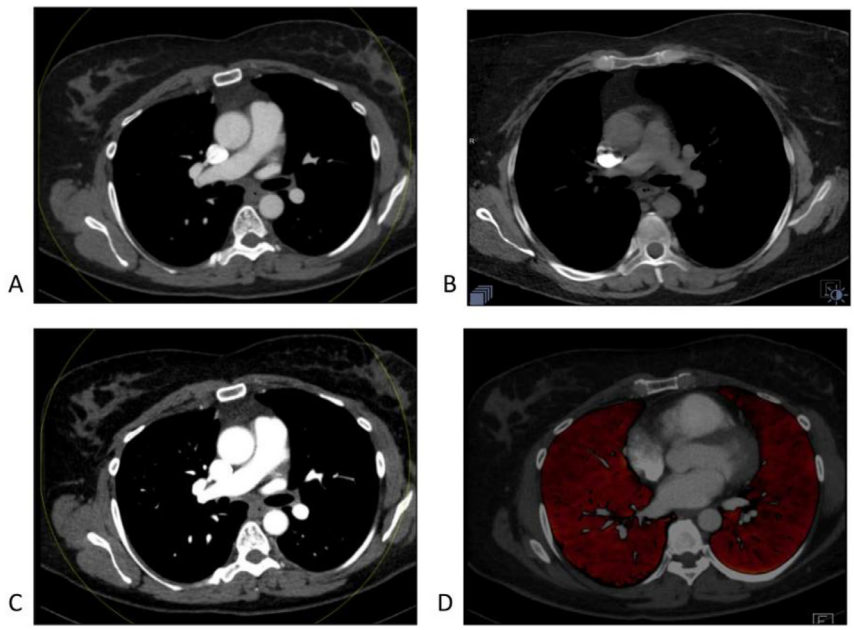

FIG 10. Example of standard dual energy reconstructions and post processing for a CT angiogram of the pulmonary arteries. (A) Mixed or linear blend images using a ratio of ≥0.6 to improve on contrast to noise ratio of single energy 120 kV. (B) Virtual Non-contrast axial dataset to show calcifications. Note that not all signal from the iodine contrast has been removed from the superior vena cava due to its high intensity. (C) Virtual monoenergetic images at 50 keV increase the iodine enhancement. This reconstruction can be helpful when iodine contrast bolus is suboptimal. (D) Perfused blood volume displays are a colored graphical way to show defects in lung perfusion.

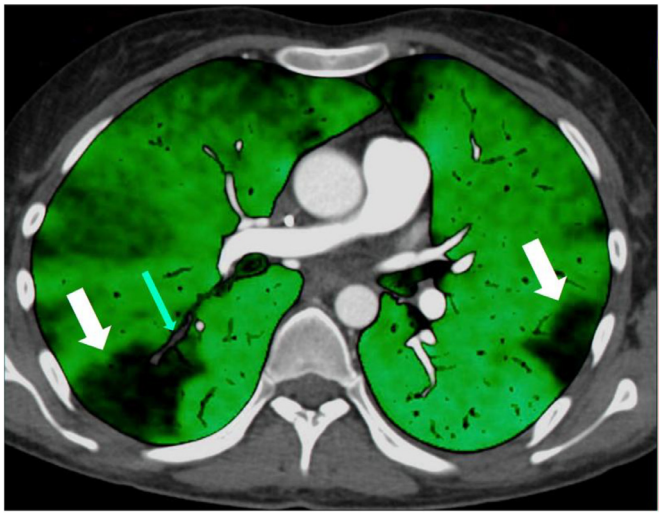

FIG 11. Twenty-six-year-old female acquired a pulmonary embolism while undergoing treatment for undifferentiated pleomorphic sarcoma. Light green arrow shows a filling defect in a right lower lobe segmental pulmonary artery, consistent with an embolus. White arrows show portions of the lungs that are not perfused due to the emboli. (Color version of figure is available online.)

settings used to reduce beam hardening artifacts. In dual energy scanning, it should be recognized that acquisition technique, image reconstruction, and patient size may cause artifacts: motion artifacts caused by slower tube rotation time; beam hardening artifacts can be caused by bones and dense contrast on low keV images; large patients may result in inferior image quality due to tube current limitations at low tube energies (Fig 10).[24]

A unique type of dual energy reconstruction is used in chest CT, called the perfused blood volume maps.[25] Perfused blood volume maps created from dual energy CT correlate with segmental and chronic pulmonary emboli seen at CT pulmonary angiography, and may improve detection of small pulmonary emboli (Fig 11).[26-28] Quantification of pulmonary perfusion from perfused blood volume maps may improve assessment of severity and risk of right heart strain.[29,30]

Clinical CT images are routinely reconstructed using an imaging matrix of 512 × 512. A larger matrix (eg, 1024 × 1024) reduces the partial volume effect for fine anatomical structures such as airway walls and interstitial markings such as the boundary of the secondary pulmonary lobule.[31] High-resolution lung imaging with larger matrix may result in improved accuracy (Fig 12), reproducibility; and for some algorithms, speed of postprocessing since the program does not have to spend as much time delineating ill-defined boundaries. Additionally, it may make subjective measurements more efficient and reproducible by minimizing partial volume affects and improving boundary recognition. Although the larger matrix size requires a greater amount of storage space, with technological improvements, larger storage is readily available.

Postprocessing in Thoracic Imaging

Computer-Aided Detection

CAD algorithms for thoracic CT generally focus on lung nodule detection. Algorithms process thin-section CT images and identify potential nodules for radiologist evaluation. Studies have shown that CAD improves pulmonary nodule detection sensitivity and compensates for deficient reader performance (Fig 13).[32,33] In addition, CAD works well with low dose CT, various scanning parameters and reconstruction methods.[34,35] In addition to automated nodule detection, more advanced CAD systems can automatically obtain nodule measurements and some even perform automated nodule matching whereby nodules identified on a follow up exam are compared to those seen on a prior study, significantly decreasing interpretation time.[36]

Lung Nodule Analysis

Nodule size is an important characteristic that dictates surveillance. The Dutch–Belgian randomized (NELSON) lung cancer screening trial was conducted based on 3-dimension volumetric measurements and raised the question of whether volumetry should play a role in nodule surveillance. Volumetric assessment of a nodule can be performed based on diameter measurements or by direct segmentation and calculation from pixel size data. Less reproducibility and precision were observed in several studies for small nodules on the order of 5 mm or less because of the increased percentage of surface area voxels in relationship to the overall nodule volume, which increased partial volume artifact.[37-39] However, it has been shown in large clinical trials that nodules less than 5 mm tend to be benign, even in the high-risk population.[40]

Several studies have shown that volumetry achieves significantly less interobserver variance compared to diameter measurements and advanced volumetry algorithms are independent of observer

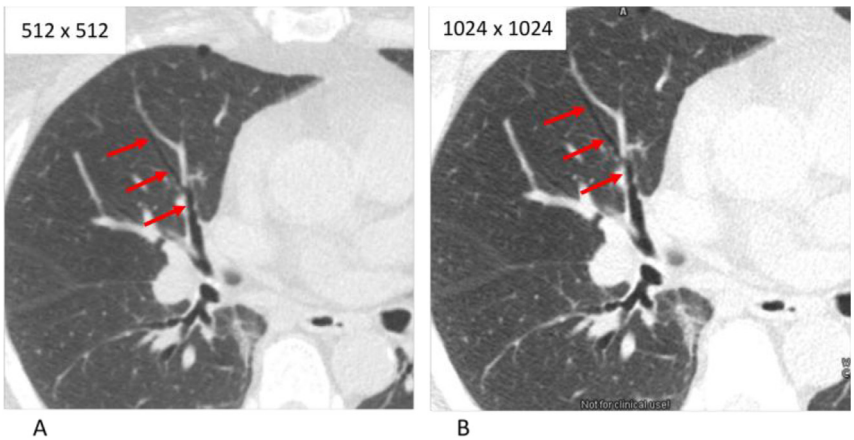

FIG 12. (A) Typical 1.5 mm slice reconstruction using a medium sharp B46 kernel and 512 × 512 matrix. (B) Corresponding CT image reconstructed using a 1024 × 1024 matrix and B46 kernel.

The spatial resolution is nearly doubled, permitting markedly improved visualization of a right middle lobe bronchus (red arrows). (Color version of figure is available online.)

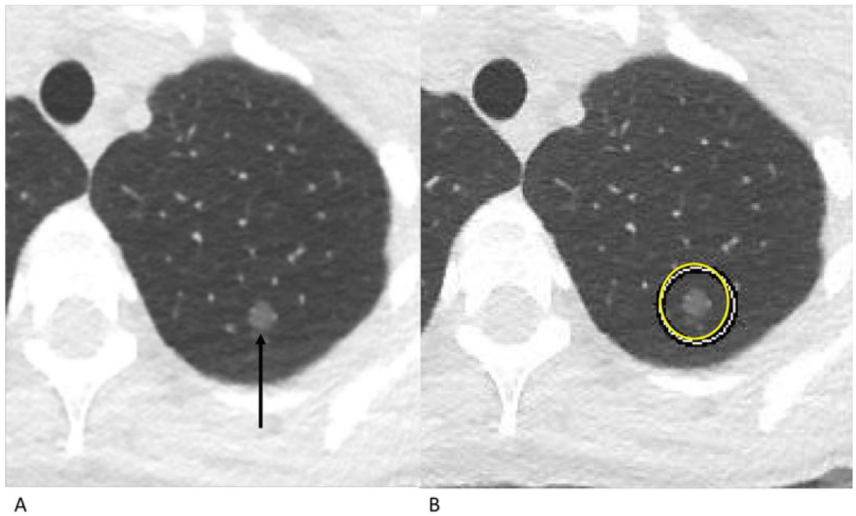

FIG 13. Forty-eight-year-old female with a history of sarcoma scanned using an ultra low radiation dose (100 kV with a tin filter and CTDIvol of 0.21 mGy) technique. The left upper lobe pure ground glass nodule was missed by the radiologist (A- black arrow) but found by CAD (B- yellow circle). (Color version of figure is available online.)

experience,[41,42] with reproducibility and accuracy preserved even with different dose settings and iterative reconstruction, which is often used for low dose or ultra-low-dose settings.[43-48] According to Knoss et al, density measurements based on volumetry are more robust than regular 2-dimension measurements. In addition to solid nodules, studies have demonstrated usefulness of volumetry for subsolid nodules.[49,50] Although volumetry has become robust enough to be considered for clinical integration, there are pitfalls that one needs to be aware when using volumetric measurement to follow nodule growth.[51] It has been shown that contrast use, reconstruction techniques and scanning parameters (eg, slice thickness), inspiratory effort, and radiation dose need to be similar between baseline and follow up scans, and it is advisable for the radiologist to review the segmentation of nodules to assure segmentation quality.[52] Moreover, de Hoop et al have shown that mean nodule volume can differ significantly between different software packages within the same vendor as well as between different vendors; therefore, it is recommended that one utilize the same segmentation algorithm and software for initial and follow-up measurements.[53]

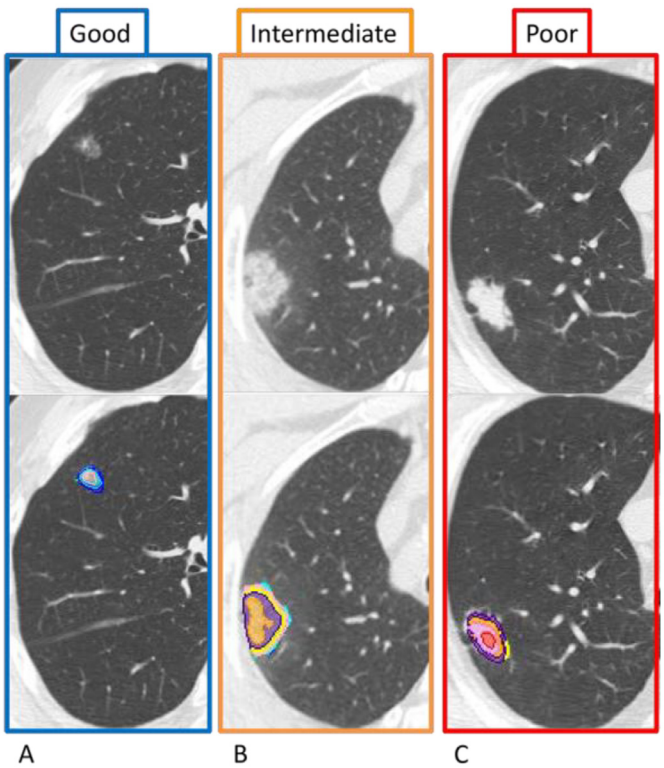

FIG 14. Computer-Aided Nodule Analysis and Risk Yield (CANARY) is a quantitative nodule analysis software that uses machine learning methodology and automated histogram analysis to characterize primary lung adenocarcinoma. The CANARY features have been shown to correlate with histologic invasiveness and overall postoperative survival for lung cancer in the adenocarcinoma spectrum. In these 3 cases, nodules in the adenocarcinoma spectrum are classified into Good (A), Intermediate (B) and Poor (C) predicted outcome, respectively. The "Good" CANARY class nodule is nearly completely ground glass density, while the "Intermediate" is mixed ground glass and solid and the "Poor" is completely solid.

Postprocessing algorithms can be used to segment lung nodules from the parenchyma and perform parametric analysis of density features that can be used as biomarkers to characterize lung nodules and stratify risk of adenocarcinoma along the spectrum of pulmonary malignancy. One such example is the Computer-Aided Nodule Analysis and Risk Yield (CANARY) algorithm (Fig 14). CANARY is a quantitative nodule analysis software that uses machine learning methodology and automated histogram analysis to characterize primary lung adenocarcinoma. Thin section CT images are then evaluated for similarity against known imaging features in the CANARY database that correlate with histologic aggressiveness and to predict patient risk.[54,55] In the future such algorithms may guide limited lung resection, or choice for localized therapeutic options (eg, radiofrequency ablation, cryo-ablation, stereotactic body radiation therapy, or proton beam therapy) vs standard surgical lobectomy or watchful waiting. Such algorithms are limited to patient populations that are relevant to their development (eg, CANARY was developed evaluating nodules in the adenocarcinoma spectrum, so would not be applicable to other types of lung cancer).

Lung Parenchyma and Pathology

Other algorithms have been developed to evaluate the pulmonary parenchyma. Computer-aided lung informatics for pathology evaluation and rating (CALIPER) is an example of a software algorithm that classifies and quantifies radiomic features of lung parenchyma on volumetric high-resolution CT scans. Radiomics refers to the analysis of quantitative image features combined with patient characteristics to provide predictive data or aid in decision support.[56] Extracted imaging features typically arise in portions of CT images associated with imaging findings of a tumor or disease, which can be detected automatically, or which could be segmented or identified by a radiologist or technologist. CALIPER and CANARY

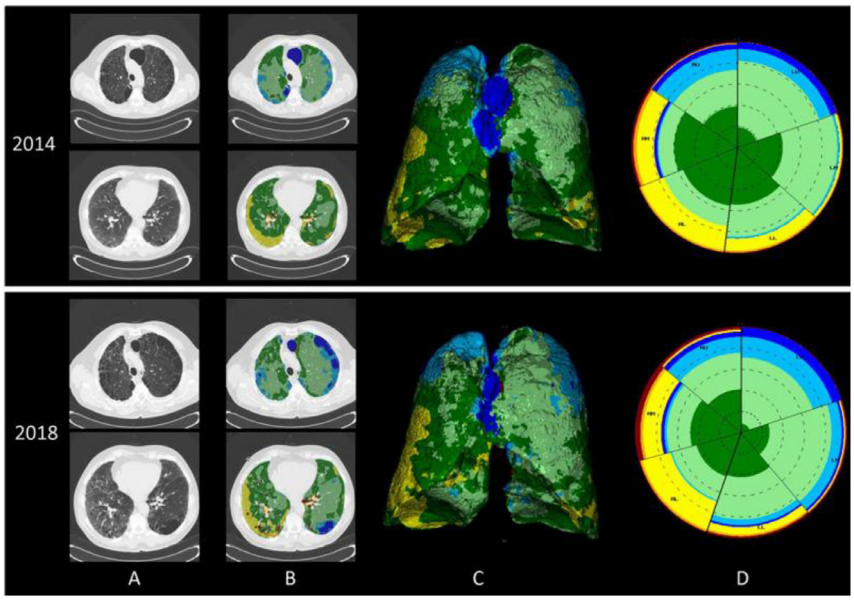

FIG 15. CALIPER (Computer-aided Lung Informatics for Pathology Evaluation and Rating) is software that performs automated anatomical segmentation and parenchymal analysis of CT image data. Based on exemplars generated by consensus evaluation of thoracic radiologists from pathologically proven cases, CALIPER classification uses histogram signatures and morphologic features of the CT image data to classify the type of parenchyma. The software characterizes each pixel as normal parenchyma (green), low attenuation (blue), ground glass opacity (yellow), reticular densities (orange) or honeycombing (red). These objectively determined parenchymal characteristics can be used to evaluate the extent and type of disease at a single timepoint as well as change over time. In complex or mixed parenchymal disease such as this case of combined pulmonary fibrosis and emphysema, the extent of each component can be evaluated and tracked longitudinally. Column A is the CT data. Column B is the parenchymal classification by CALIPER algorithms. Column C is a 3D rendering of the parenchymal features of the lungs. Column D is a glyph representing the regional extent of the classified parenchyma. In this specific case, the extent of fibrosis has increased over time, the character of fibrosis has become more reticular with more honeycombing and regional volume loss in the lung bases while at the same time the emphysema/bullae in the upper lungs has also increased in extent and volume. (Color version of figure is available online.)

are examples of a number of growing radiomic algorithms. CALIPER has been shown to aid in diagnosing and prognosing early pulmonary parenchymal disease and in follow up to determine disease progression or treatment response (Fig 15).[57-59] The algorithm automatically characterizes and quantifies diffuse pulmonary parenchymal abnormalities or low attenuation disease such as emphysema or air trapping, and can be used to objectively monitor progression or response to treatment over time, or in guiding treatment options. This is important, in part, as distinct chronic obstructive pulmonary disease phenotypes have been described, which have management and risk implications.[60] For example, upper-lobe predominant emphsyma is a COPD phenotype that can be treated with surgical lung volume reduction, and can be evaluated and followed quantitatively with CALIPER type algorithms.

Dual-Energy Thoracic CT Angiography (CTA)

Dual-energy information is postprocessed to provide virtual noncontrast, iodine only, and virtual monoenergetic images, and perfused blood volume maps, and has been explained earlier. Currently such postprocessing is performed differently with specific CT vendor workstations, with automatic or manual postprocessing of images by technologists, or with data viewed interactively by radiologists on vendor-specific workstations. Clinical efficiency and access of such postprocessed images is needed for radiologists to incorporate the benefit of the additional information provided from dual energy images.

Conclusion

Multiple new CT acquisition and reconstruction techniques, along with advanced postprocessing methods have brought us closer to personalized CT examination. Such recent innovations have breathed new life into an era of more efficient and detailed analysis of changes in pulmonary architecture and function.

Acknowledgments

The authors would like to thank Dr. Yong Suk Lee, Lori L. Peterson, RT and Cynthia F. Walfoort, RT for their input and assistance, as well as Kristina Nunez, for assistance in manuscript preparation.

Supplementary materials

Supplementary material associated with this article can be found in the online version at doi:10.1067/j.cpradiol.2018.10.003.

References

1. Marin D, Boll DT, Mileto A, Nelson RC. State of the art: Dual-energy CT of the abdomen. Radiology 2014;271:327–42.
2. McCollough CH, Leng S, Yu L, Fletcher JG. Dual- and multi-energy CT: Principles, technical approaches, and clinical applications. Radiology 2015;276:637–53.
3. Flohr TG, Leng S, Yu L, et al. Dual-source spiral CT with pitch up to 3.2 and 75 ms temporal resolution: Image reconstruction and assessment of image quality. Med Phys 2009;36:5641–53.
4. Gordic S, Morsbach F, Schmidt B, et al. Ultralow-dose chest computed tomography for pulmonary nodule detection: First performance evaluation of single energy scanning with spectral shaping. Invest Radiol 2014;49:465–73.
5. Weis M, Henzler T, Nance JW Jr., et al. Radiation dose comparison between 70 kVp and 100 kVp with spectral beam shaping for non-contrast-enhanced pediatric chest computed tomography: A prospective randomized controlled study. Invest Radiol 2017;52:155–62.
6. Alvarez RE, Macovski A. Energy-selective reconstructions in X-ray computerized tomography. Phys Med Biol 1976;21:733–44.
7. Primak AN, Ramirez Giraldo JC, Liu X, et al. Improved dual-energy material discrimination for dual-source CT by means of additional spectral filtration. Med Phys 2009;36:1359–69.
8. Barrett JF, Keat N. Artifacts in CT: Recognition and avoidance. Radiographics 2004;24:1679–91.
9. Hagelstein C, Henzler T, Haubenreisser H, et al. Ultra-high pitch chest computed tomography at 70 kVp tube voltage in an anthropomorphic pediatric phantom and non-sedated pediatric patients: Initial experience with 3(rd) generation dual-source CT. Z Med Phys 2016;26:349–61.
10. Hou DJ, Tso DK, Davison C, et al. Clinical utility of ultra high pitch dual source thoracic CT imaging of acute pulmonary embolism in the emergency department: Are we one step closer towards a non-gated triple rule out? Eur J Radiol 2013;82:1793–8.

11. Flohr TG, Bruder H, Stierstorfer K, et al. Image reconstruction and image quality evaluation for a dual source CT scanner. Med Phys 2008;35:5882–97.
12. Newell JD Jr., Fuld MK, Allmendinger T, et al. Very low-dose (0.15 mGy) chest CT protocols using the COPDGene 2 test object and a third-generation dual-source CT scanner with corresponding third-generation iterative reconstruction software. Invest Radiol 2015;50:40–5.
13. Geyer LL, Schoepf UJ, Meinel FG, et al. State of the art: Iterative CT reconstruction techniques. Radiology 2015;276:339–57.
14. Gierada DS, Bierhals AJ, Choong CK, et al. Effects of CT section thickness and reconstruction kernel on emphysema quantification relationship to the magnitude of the CT emphysema index. Acad Radiol 2010;17:146–56.
15. Wang Y, de Bock GH, van Klaveren RJ, et al. Volumetric measurement of pulmonary nodules at low-dose chest CT: Effect of reconstruction setting on measurement variability. Eur Radiol 2010;20:1180–7.
16. Strub WM, Weiss KL, Sun D. Hybrid reconstruction kernel: Optimized chest CT. AJR Am J Roentgenol 2007;189:W115–6.
17. Angelelli G, Grimaldi V, Spinelli F, et al. Multi slice computed tomography in the study of pulmonary metastases. Radiol Med 2008;113:954–67.
18. Kawel N, Seifert B, Luetolf M, Boehm T. Effect of slab thickness on the CT detection of pulmonary nodules: Use of sliding thin-slab maximum intensity projection and volume rendering. AJR Am J Roentgenol 2009;192:1324–9.
19. Kilburn-Toppin F, Arthurs OJ, Tasker AD, Set PA. Detection of pulmonary nodules at paediatric CT: Maximum intensity projections and axial source images are complementary. Pediatr Radiol 2013;43:820–6.
20. Park EA, Goo JM, Lee JW, et al. Efficacy of computer-aided detection system and thin-slab maximum intensity projection technique in the detection of pulmonary nodules in patients with resected metastases. Invest Radiol 2009;44:105–13.
21. Thieme SF, Johnson TR, Lee C, et al. Dual-energy CT for the assessment of contrast material distribution in the pulmonary parenchyma. AJR Am J Roentgenol 2009;193:144–9.
22. Yu L, Primak AN, Liu X, McCollough CH. Image quality optimization and evaluation of linearly mixed images in dual-source, dual-energy CT. Med Phys 2009;36:1019–24.
23. Kang MJ, Park CM, Lee CH, et al. Dual-energy CT: clinical applications in various pulmonary diseases. Radiographics 2010;30:685–98.
24. Guimaraes LS, Fletcher JG, Harmsen WS, et al. Appropriate patient selection at abdominal dual-energy CT using 80 kV: Relationship between patient size, image noise, and image quality. Radiology 2010;257:732–42.
25. Krissak R, Henzler T, Reichert M, et al. Enhanced visualization of lung vessels for diagnosis of pulmonary embolism using dual energy CT angiography. Invest Radiol 2010;45:341–6.
26. Lu GM, Wu SY, Yeh BM, Zhang LJ. Dual-energy computed tomography in pulmonary embolism. Br J Radiol 2010;83:707–18.
27. Lu GM, Zhao Y, Zhang LJ, Schoepf UJ. Dual-energy CT of the lung. AJR Am J Roentgenol 2012;199:S40–53.
28. Zhang LJ, Zhao YE, Wu SY, et al. Pulmonary embolism detection with dual-energy CT: Experimental study of dual-source CT in rabbits. Radiology 2009;252:61–70.
29. Sakamoto A, Sakamoto I, Nagayama H, et al. Quantification of lung perfusion blood volume with dual-energy CT: Assessment of the severity of acute pulmonary thromboembolism. AJR Am J Roentgenol 2014;203:287–91.
30. Zhang LJ, Yang GF, Zhao YE, et al. Detection of pulmonary embolism using dual-energy computed tomography and correlation with cardiovascular measurements: a preliminary study. Acta Radiol 2009;50:892–901.
31. Hata A, Yanagawa M, Honda O, et al. Effect of matrix size on the image quality of ultra-high-resolution CT of the lung: Comparison of 512 x 512, 1024 x 1024, and 2048 x 2048. Acad Radiol 2018;25:869–76.
32. Marten K, Engelke C, Seyfarth T, et al. Computer-aided detection of pulmonary nodules: Influence of nodule characteristics on detection performance. Clin Radiol 2005;60:196–206.
33. Rubin GD, Lyo JK, Paik DS, et al. Pulmonary nodules on multi-detector row CT scans: Performance comparison of radiologists and computer-aided detection. Radiology 2005;234:274–83.
34. Lee JY, Chung MJ, Yi CA, Lee KS. Ultra-low-dose MDCT of the chest: Influence on automated lung nodule detection. Korean J Radiol 2008;9:95–101.
35. Wielputz MO, Wroblewski J, Lederlin M, et al. Computer-aided detection of artificial pulmonary nodules using an ex vivo lung phantom: Influence of exposure parameters and iterative reconstruction. Eur J Radiol 2015;84:1005–11.
36. Koo CW, Anand V, Girvin F, et al. Improved efficiency of CT interpretation using an automated lung nodule matching program. AJR Am J Roentgenol 2012;199:91–5.
37. Goo JM, Tongdee T, Tongdee R, et al. Volumetric measurement of synthetic lung nodules with multi-detector row CT: effect of various image reconstruction parameters and segmentation thresholds on measurement accuracy. Radiology 2005;235:850–6.
38. Kostis WJ, Yankelevitz DF, Reeves AP, et al. Small pulmonary nodules: Reproducibility of three-dimensional volumetric measurement and estimation of time to follow-up CT. Radiology 2004;231:446–52.
39. Petrou M, Quint LE, Nan B, Baker LH. Pulmonary nodule volumetric measurement variability as a function of CT slice thickness and nodule morphology. AJR Am J Roentgenol 2007;188:306–12.
40. Bartholmai BJ, Koo CW, Johnson GB, et al. Pulmonary nodule characterization, including computer analysis and quantitative features. J Thorac Imaging 2015;30:139–56.
41. Bolte H, Jahnke T, Schafer FK, et al. Interobserver-variability of lung nodule volumetry considering different segmentation algorithms and observer training levels. Eur J Radiol 2007;64:285–95.
42. Koike W, Iwano S, Matsuo K, et al. Doubling time calculations for lung cancer by three-dimensional computer-aided volumetry: Effects of inter-observer differences and nodule characteristics. J Med Imaging Radiat Oncol 2014;58:82–8.
43. Doo KW, Kang EY, Yong HS, et al. Accuracy of lung nodule volumetry in low-dose CT with iterative reconstruction: An anthropomorphic thoracic phantom study. Br J Radiol 2014;87:20130644.
44. Hein PA, Romano VC, Rogalla P, et al. Variability of semiautomated lung nodule volumetry on ultralow-dose CT: Comparison with nodule volumetry on standard-dose CT. J Digit Imaging 2010;23:8–17.
45. Kim H, Park CM, Song YS, et al. Influence of radiation dose and iterative reconstruction algorithms for measurement accuracy and reproducibility of pulmonary nodule volumetry: A phantom study. Eur J Radiol 2014;83:848–57.
46. Knoss N, Hoffmann B, Fabel M, et al. Lung nodule assessment in computed tomography: Precision of attenuation measurement based on computer-aided volumetry. Rofo 2009;181:1151–6.
47. Wielputz MO, Lederlin M, Wroblewski J, et al. CT volumetry of artificial pulmonary nodules using an ex vivo lung phantom: Influence of exposure parameters and iterative reconstruction on reproducibility. Eur J Radiol 2013;82:1577–83.
48. Xie X, Willemink MJ, Zhao Y, et al. Inter- and intrascanner variability of pulmonary nodule volumetry on low-dose 64-row CT: An anthropomorphic phantom study. Br J Radiol 2013;86:20130160.
49. Kim H, Park CM, Lee SM, et al. A comparison of two commercial volumetry software programs in the analysis of pulmonary ground-glass nodules: Segmentation capability and measurement accuracy. Korean J Radiol 2013;14:683–91.
50. Oda S, Awai K, Murao K, et al. Computer-aided volumetry of pulmonary nodules exhibiting ground-glass opacity at MDCT. AJR Am J Roentgenol 2010;194:398–406.
51. Devaraj A, van Ginneken B, Nair A, Baldwin D. Use of volumetry for lung nodule management: Theory and practice. Radiology 2017;284:630–44.
52. Koo CW. Advanced imaging tools in pulmonary nodule detection and surveillance. Clin Imaging 2016;40:296–301.
53. de Hoop B, Gietema H, van Ginneken B, et al. A comparison of six software packages for evaluation of solid lung nodules using semi-automated volumetry: What is the minimum increase in size to detect growth in repeated CT examinations. Eur Radiol 2009;19:800–8.
54. Maldonado F, Duan F, Raghunath SM, et al. Noninvasive computed tomography-based risk stratification of lung adenocarcinomas in the National Lung Screening Trial. Am J Respir Crit Care Med 2015;192:737–44.
55. Raghunath S, Maldonado F, Rajagopalan S, et al. Noninvasive risk stratification of lung adenocarcinoma using quantitative computed tomography. J Thorac Oncol 2014;9:1698–703.
56. Gillies RJ, Kinahan PE, Hricak H. Radiomics: Images are more than pictures, they are data. Radiology 2016;278:563–77.
57. Jacob J, Bartholmai BJ, Rajagopalan S, et al. Functional and prognostic effects when emphysema complicates idiopathic pulmonary fibrosis. Eur Respir J 2017;50(1):1700379.
58. Jacob J, Bartholmai BJ, Rajagopalan S, et al. Automated quantitative computed tomography versus visual computed tomography scoring in idiopathic pulmonary fibrosis: Validation against pulmonary function. J Thorac Imaging 2016;31:304–11.
59. Maldonado F, Moua T, Rajagopalan S, et al. Automated quantification of radiological patterns predicts survival in idiopathic pulmonary fibrosis. Eur Respir J 2014;43:204–12.
60. Misra S, Benzo R. Chronic obstructive pulmonary disease phenotypes: Implications for care. Mayo Clin Proc 2017;92:1104–12.